Discovery of Ag_xTaS_2 Superconductor with Stage-3 Structure

Khurelbaatar Zagarzusem[1,2], Masaya Fujioka[1*], Taizo Shibuya[3], Satoshi Demura[4], Shintaro Adachi[5], Yoshihiko Takano[5], Melbert Jeem[1], Madoka Ono[1,6], Hideo Kaiju[7] and Junji Nishii[1]

[1] Research Institute for Electronic Science, Hokkaido University, N20W10, Sapporo 001-0020, Japan
[2] Department of Electronics, School of Information and Communication Technology, Mongolian University of Science and Technology, Ulaanbaatar 14191, Mongolia
[3] System Platform Research Laboratories, NEC Corporation, Tsukuba, Ibaraki 305-8501, Japan
[4] College of Science and Technology, Nihon University, 1-8-14 Surugadai, Kanda, Chiyoda-ku, Tokyo 101–8308, Japan
[5] MANA, National Institute for Materials Science, 1-2-1 Sengen, Tsukuba, Ibaraki 305-0047, Japan
[6] Materials Integration Laboratories, AGC Inc., 1150 Hazawa-cho, Kanagawa-ku Yokohama, Kanagawa 221-8755, Japan
[7] Department of Applied Physics and Physico-Informatics, Faculty of Science and Technology, Keio University, Yokohama, Kanagawa 223-8522, Japan

E-mail: fujioka@ es.hokudai. ac.jp

Received xxxxxx
Accepted for publication xxxxxx
Published xxxxxx

Abstract

Through interfacial engineering, such as ion intercalation, we can tune the properties and optimize the performance of transition metal dichalcogenides and their devices. In this study, we present the first-time experimental investigations of stage 3 of Ag_xTaS_2 single crystal, and its superconductivity was discovered at 3.8 K. Highly crystalline stage 1 and 2 were prepared by a proton-driven ion-introduction method. A simple water-soaking process was employed to achieve the stage-3 structure by deintercalation of Ag ions from lower stage structures. Besides, we developed a general stacking rule to determine the crystal structure, and it can predict any higher-order stage structure of Ag_xTaS_2. The superconducting transition temperature was enhanced from 1.7 K for a stage-2 structure to 3.8 K for a stage-3 structure, which is more than four times that of the pristine TaS_2 (0.8 K). This enhancement is attributed to the increase in density of states at the Fermi level, which was calculated by density functional theory. Also, the water-soaking process reconstructs the stage-2 into the stage-3 structure while deteriorating its crystallinity. Such a structural distortion is one of the potential reasons for the suppression of charge density wave in stage-2, resulting in the enhancement of superconductivity despite the structural degradation.

Keywords: Two-dimensional tantalum disulfide, Stage structure, Intercalation, Superconductivity, Charge density wave, Solid-state electrochemistry, Density functional theory

1. Introduction

Two-dimensional (2-D)-layered transition metal dichalcogenides (TMDs) have recently attracted a lot of interest due to their various physical phenomenon and outstanding properties for next-generation electronics and optoelectronic applications [1–4]. In comparison with homogeneous monolayers, layered TMDs exhibit more degrees of freedom because of the covalent bonding within each layer and the van der Waals (vdW) interactions between the layers. This weak vdW interaction between the layers allows the penetration of various foreign species, such as alkali metal ions, transition metals, and even organic molecules, into the crystal, forming intercalated compounds. Along with this intercalation process, a “staging” phenomenon occurs, i.e., the introduced atoms tend to periodically penetrate the layers of the host material through the *c*-axis. The number of host layers sandwiched between the two layers of the introduced atoms is referred to as the

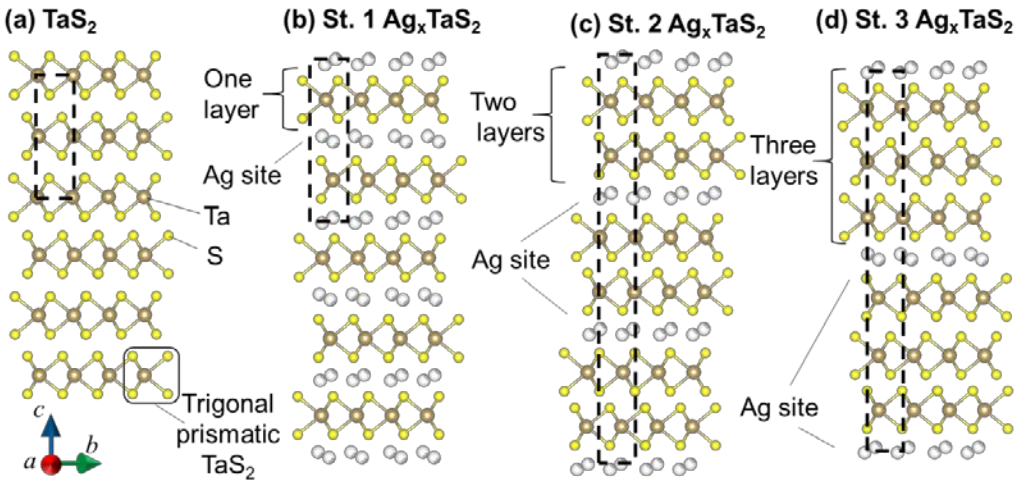

Figure 1. Systematic illustrations (side view) of the crystal structures of (a) TaS_2, (b) Ag_xTaS_2 with stage 1, (c) Ag_xTaS_2 with stage 2, and (d) Ag_xTaS_2 with stage 3. Notations: Ta atoms are shown in brown and S atoms in yellow. Trigonal prismatic geometry is highlighted by the red polyhedron. The introduced Ag ion sites are shown in grey. The dashed rectangles show the unit cell of each structure.

stage number and the resultant structures are named as stage-1, stage-2, stage-3, etc [5]. The occurrence of well-ordered higher stages (greater than 2) is very common in graphite intercalation compounds; up to 10 stages have been observed for graphite intercalates [6].

Although such a staging phenomenon is also observed in many other intercalated compounds, most of the scientific effort so far has focused on those of graphite [7, 8]. Layered TMDs generally do not exhibit accurate staging. Hence, direct observation of staging has remained a challenging issue. Despite the substantial research attention that has been directed to the intercalation phenomena for layered TMDs, many fundamental questions remain unanswered. Thus, further exploration is needed.

Tantalum disulfate (TaS_2), an example of layered TMDs with a quasi-2-D structure, is considered a good candidate for investigating the novel properties of intercalated materials. It exists in many different polytype forms, depending on the orientation of the sulfur (S) atoms, which are covalently bonded to the tantalum (Ta) atoms. Such orientations include trigonal 1T-TaS_2, double-layer hexagonal 2H-TaS_2, rhombohedral 3R-TaS_2, 1T and 2H stacking structured 4Hb-TaS_2, and mixed coordination 6R-TaS_2 [9–12]. Among these polytypes, the 2H-TaS_2 shows both superconductivity and charge density wave (CDW) transitions and also has good stability in organic and inorganic intercalation [13]. Thus, 2H-TaS_2 has attracted significant attention. It exhibits a CDW phase at 78 K and a superconducting transition temperature (T_c) of 0.8 K [14, 15].

Monovalent silver (Ag) ions are generally considered very suitable for the intercalation of TaS_2 due to their high mobility, preferred structural sites, and good interactions with the neighboring atoms [16]. Therefore, studies have been carried out to investigate the crystal structure, CDW formation, superconducting properties, and electrical properties of Ag_xTaS_2, as well as on the chemical diffusivity of Ag and the associated activation energy for mobility [17–21]. Although Ag-intercalated TaS_2 has been extensively studied, it remains a difficult task to achieve the formation of stage-3 structure in comparison with stage-1 and stage-2 structures.

Figure 1 illustrates the crystal structures of pristine TaS_2 and intercalated Ag_xTaS_2 with stage-1 to stage-3 structures. The unit cell of pure 2H-TaS_2 consists of two TaS_2 layers. Each layer is formed by Ta atoms surrounded by six S atoms arranged in a hexagonal symmetric trigonal prismatic coordination (figure 1(a)). Depending on the mole fraction value of x, it is possible to obtain various stages in Ag_xTaS_2 structures, just as in graphite. A stage-1 structure with $x = 0.67$ was described first by Van de Berg [22]. In the stage-1 Ag_xTaS_2 structure, the vdW gap between the TaS_2 layers is filled by Ag ions; thus the maximum content of Ag is obtained in this stage (figure 1(b)). In the stage-2 Ag_xTaS_2 structure, the unit cell contains six TaS_2 layers, every pair being sandwiched by Ag sites (figure 1(c)). A stage-2 structure was observed when $x \approx 0.33$, which is in good agreement with several other studies [18]. In the stage-3 Ag_xTaS_2 structure, the number of TaS_2 layers in the unit cell is the same as that in stage 2, but every three TaS_2 layers are filled by Ag (figure 1(d)). The existence of stage 3 was predicted 40 years ago by Scholtz and Frindt [23]. Also, in 1988, Weigers et al. demonstrated the difficulty in the synthesis of stage 3 through some thermodynamical analysis. They concluded that the mixture of stage-2 and 2H-TaS_2 is more stable than the stage-3 structure. Hence, it is thought to

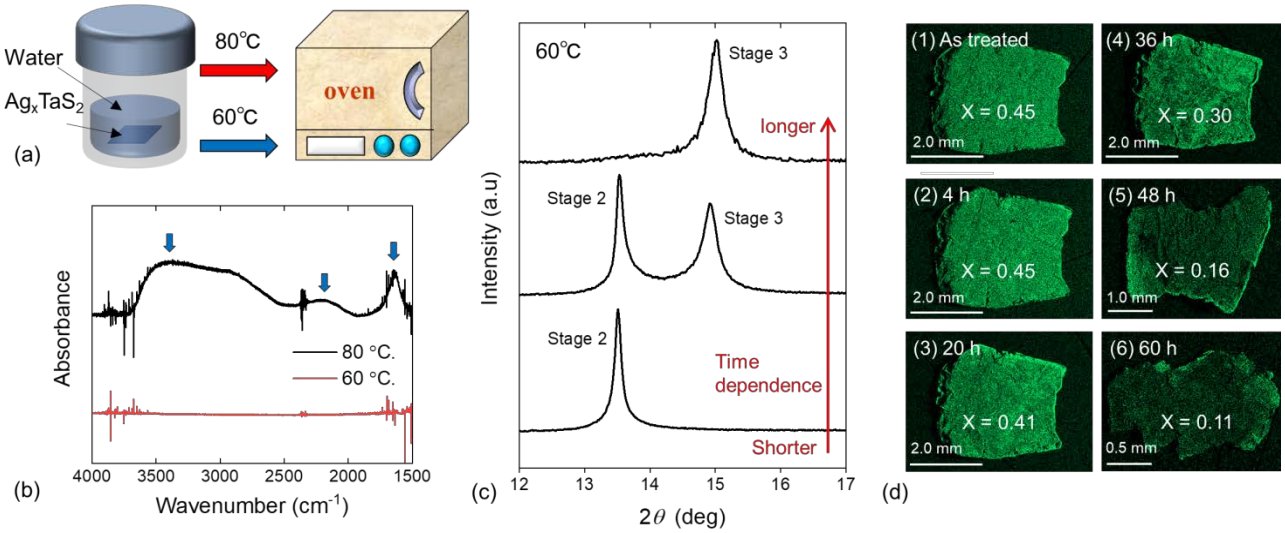

Figure 2. (a) Schematic of the experimental process. (b) IR spectra of the water molecules in the interlayers of Ag_xTaS_2 treated at 60 ºC and 80 ºC. (c) XRD patterns for time dependence of water soaking process from stage-2 structured Ag_xTaS_2 at 60 ºC (d) Variation of Ag^+ concentration at various treatment time.

be the reason why there are no reports about the experimental investigation of stage-3-structured Ag_xTaS_2.

In this study, we achieved an almost single-phased stage-3 structure (94 wt%) and performed first-time experimental investigations. Also, first-principles calculations based on density functional theory (DFT) was employed to gain insight into the experimental observations. Previously, we discovered the superconductivity of a single-crystalline Ag_xTaS_2 (x = 0.45, 0.21) with stage-1 and stage-2 structures using the liquid-free proton-driven ion-introduction (PDII) method [24]. As a continuation of our previous work, herein, we report the fabrication process, structural characterization, and physical properties of stage-3 Ag_xTaS_2 single crystals. In particular, the relationship between the previously reported CDW in stage-2 and the superconductivity enhancement observed in stage-3 was discussed.

Furthermore, since the stage-3 structure of Ag_xTaS_2 was obtained only via the liquid-phase process, the samples were not highly crystalline and were cleaved to small pieces during the process. Thus, it is difficult to determine their in-plane structures due to the insignificant intensity. However, the obtained highly oriented 00*l* indexes provide information on the number of stages and crystal structure. These findings could help in the development of a general stacking rule for the system, which could explain the higher staging phenomena of Ag_xTaS_2. The developed stacking rule was found to be in excellent agreement with the *c*-lattice constant of stage-2 and -3 structured Ag_xTaS_2. Besides, we carried out DFT calculations to estimate the relative stability of the staged Ag_xTaS_2 structure.

2. Experimental Section

Typically, single-crystalline 2H-Ag_xTaS_2 ($0 \leq x \leq 0.45$) was prepared via the PDII method using a process described in our previous report [24]. The freshly prepared Ag_xTaS_2 was completely immersed in ultrapure water inside a screw reagent bottle. The samples were then annealed at 60 and 80 ºC in an oven for several hours, after which they were dried before further analysis. The chemical compositions of the obtained Ag_xTaS_2 single crystals were determined via energy dispersive spectroscopy (EDS) in a JEOL/JCM-6000 scanning electron microscope. The infrared (IR) absorption spectra were measured using the JASCO/IRT-3000N spectrophotometer. The crystal structures and phase purities of the samples were examined via X-ray diffraction (XRD) measurements using Cu Kα radiation (λ = 1.5409 Å) at room temperature. The temperature dependence of the electrical resistivity, $\rho(T)$, was measured using an adiabatic demagnetization refrigerator system (Quantum Design, Physical Property Measurement System) employing the standard four-probe technique. Also, the superconducting transition was determined via magnetic measurements using a superconducting quantum magnetometer (Quantum Design, Magnetic Property Measurement System).

The density of states (DOS) of $Ag_{24}Ta_{54}S_{108}$ with stage-1 (186 atoms), $Ag_{12}Ta_{54}S_{108}$ with stage-2 (174 atoms) and $Ag_4Ta_{54}S_{108}$ with stage-3 (166 atoms) structures were calculated using the Vienna ab-initio simulation package (VASP) based on DFT [25, 26]. The generalized gradient approximation (GGA) method was implemented in the plane-wave code [27]. Based on the DFT-D3 methods [28,29], the projector-augmented wave scheme and vdW forces were employed to estimate the interactions between the ion cores and valance electrons [30]. A cut-off energy level of 350 eV was used for the plane waves, and the

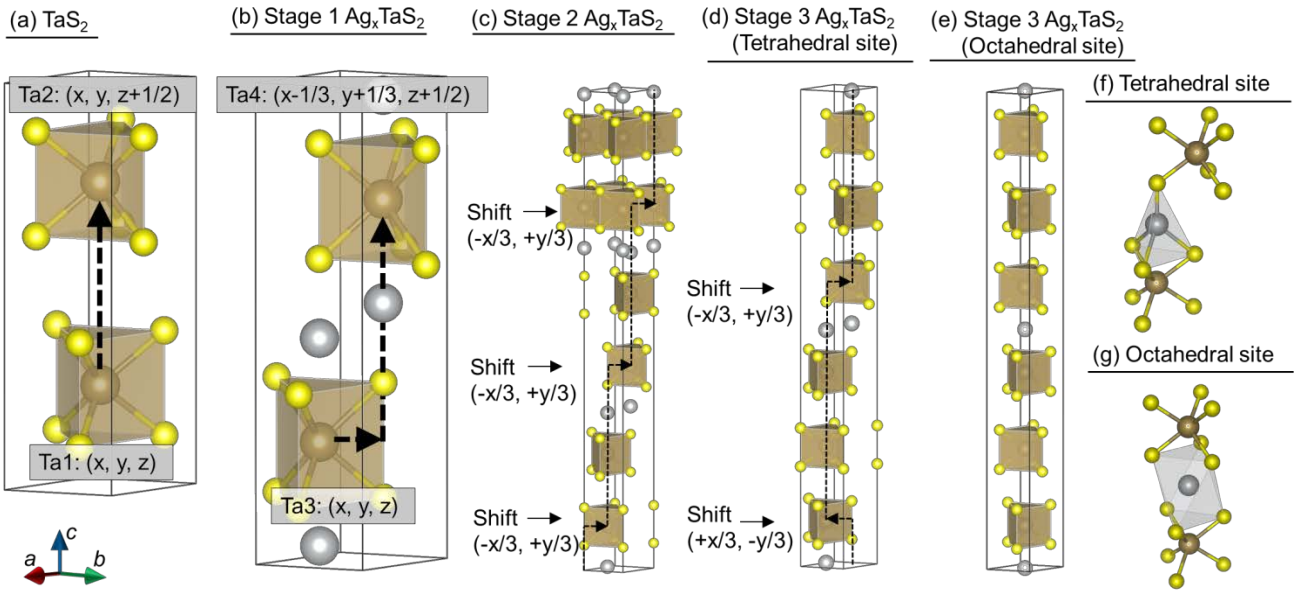

Figure 3. (a)–(e) Crystallographic illustration of TaS_2 and stage structures for Ag_xTaS_2. (f), (g) Tetrahedral site and octahedral site composed of S atoms, respectively.

Methfessel-Paxton method with a width of sigma of 0.2 eV for the occupation of the electronic level was used in the calculations. The Brillouin zone of each material was sampled with a Monkhorst-Pack k-point grid of 4 × 4 × 1. Supercells were modelled with the Ag atoms placed at the furthest site from one another. Structural relaxations were carried out to optimize all the ionic positions in each supercell.

3. Results

3.1 Water treatment

Figure 2 (a) illustrates the water-soaking process. In hot water, Ag ions were gradually discharged from the interlayers of Ag_xTaS_2. The obtained IR spectra, as well as the XRD patterns, were completely different for the samples treated at different temperatures between 60 and 80 ºC. As shown in figure 2 (b), three absorption peaks (indicated by blue arrows) of water molecules were observed in the samples treated at 80 ºC. The broad absorption band around 2500–3700 cm^{-1} and intense band at 1638 cm^{-1} are caused by O-H stretching and O-H-O scissors bending of water molecules, respectively. Also, smaller band at 2120 cm^{-1} is the result of coupling of those bands [31]. No water molecules were detected in the sample treated at 60 °C. Furthermore, the XRD patterns for Ag_xTaS_2 with a stage-2 structure and those of the samples subjected under the water-soaking process are shown in figure S1 (c). The intervals of the *c*-axis-oriented peaks are different between 60 and 80 °C. It means that a difference of only 20 °C causes a large change in the crystal structure and that the water-soaking process at 80 °C induces the co-intercalation of water molecules and Ag ions. Thus, the process is temperature-sensitive. Also, the treatment time depends on the sample size, shape, and Ag concentration. Therefore, the gradual change in structure and composition were monitored by taking the sample from hot water every four hours. Figure 2 (c) shows the process in which the XRD main peak changes from stage 2 to stage 3. The weight percentage of the stage-3 structure obtained was estimated to be 94 % by using the direct-derivation method. The detail is shown in supplemental information in figure S2. Figures 2 (d1–d6) show the treatment-time dependence of the Ag ion concentration (x) at 60 ºC. The hot water treatment effectively removed a certain amount of Ag ions from the interlayers of TaS_2, as the concentration of Ag decreased from 0.45 to 0.11 within 60 hours. The listed x values were obtained from the averages of several measurements of the EDS quantitative analysis performed at the center positions of samples. During the water-soaking process, the samples were spontaneously cleaved such that the shape displayed in figures 2 (d5) and (d6) changed from the original shape.

3.2 Crystal structure of stage-3-structured Ag_xTaS_2

Based on the unit-cell-formation mechanism of the pristine TaS_2 and stage-1 Ag_xTaS_2 crystal structures, a general stacking rule was developed to predict the formation of a higher staged-Ag_xTaS_2 structure. As shown in figure 3 (a), the unit cell of the TaS_2 formed by two trigonal prismatic units; each of the trigonal prismatic unit contains a Ta atom that sits at the center of a trigonal prismatic cage formed by six S atoms. These unit cells are repeated by sharing their

edges in the horizontal direction to form TaS_2 layers. In the upper layer, the fractional x-and y-coordinates of the Ta atoms are the same as those of the bottom Ta atom, even though the trigonal prismatic unit rotates in the reverse direction. When Ag ions were inserted into the TaS_2 layers, two possible sites emerged; the tetrahedral and octahedral sites composed of S atoms, as shown in figure 3 (f) and (g). In the reported crystal structure of stage 1 and stage 2, the tetrahedrons are formed and occupied by Ag ions. Therefore, the structure with tetrahedral sites is usually more stable than that with octahedral sites. However, when the Ag concentration is significantly diluted, the structure with octahedral sites becomes slightly more stable, as predicted from the DFT calculation (figure S7). In this study, both cases of the crystal structure for stage 3 were considered.

First, the crystal structure of stage 3 with tetrahedral sites is explained. To form the tetrahedron, the TaS_2 layer on interfacial Ag ions must be shifted parallel by −1/3 and +1/3 in the x-and y-directions, respectively. The dashed lines with directional arrows in figure 3 (a) and (b) indicate the shift in the location of the Ta atom. From this simple stacking rule, the prediction of higher-order stage structures of Ag_xTaS_2 was possible. In the case of stage-2 structure, since the Ag ions are inserted in every two TaS_2 layers, the Ta atoms would always shift in the same direction at the indicated layers by arrows in figure 3 (c) and afterward return to the original position after shifting three times. Thus, six layers are required for the stage-2 structure to form a unit cell, as shown in figure 3 (c). On the other hand, in the case of the odd-numbered stage structures, Ag ions are alternately placed on the triangular prisms with different directions. As a result, the TaS_2 layers on Ag atoms would alternately change the direction of the shifts as in stage-1 and stage-3 structures, as shown in figures 3 (b) and (d), respectively. On the other hand, when the Ag ions are located at the center of the octahedron, the crystal structure could be simpler. In such a scenario, TaS_2 layers do not show any shift so that the Ta and Ag atoms line up in a row in figure 3(e).

Figure 4 shows the XRD patterns for the pristine TaS_2, Ag-intercalated Ag_xTaS_2 with stage 1, stage 2, and stage 3. Only 00*l* reflections were observed because of their *c*-axis-preferred orientation of the plate-shaped single crystal. The XRD patterns for the pristine TaS_2 and the Ag_xTaS_2 with stage-1 and stage-2 structures are in excellent agreement with previously reported results [24]. The space groups of the designed crystal structures of stage-3 shown in figure 3(d) and 3(e) were found to be P-6 m2 and P3 m1, respectively, by using the software of Visualization for Electronic and Structural Analysis, VESTA [32]. The detailed information for the determination of the crystal structure is described in section 4 of the supporting information. The *c*-lattice parameter of the crystal structure was roughly estimated to be 36.8 Å from the total height of three components: the

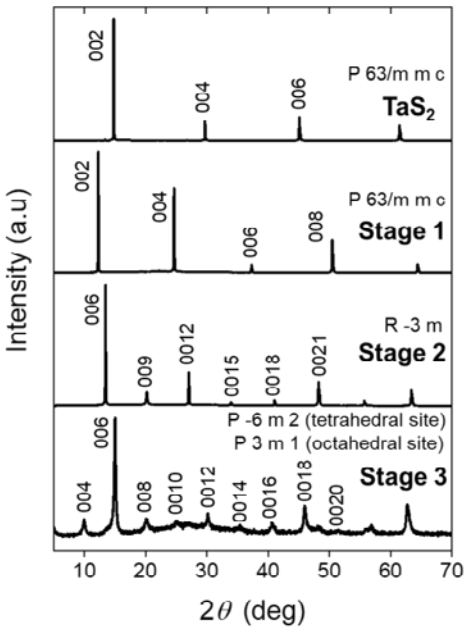

Figure 4. XRD patterns for TaS_2 and Ag_xTaS_2 with stage 1, stage 2, and stage 3.

TaS_2 layers, gaps between the layers, and the gaps including Ag ions. With the assumption that the *a*- and *b*-lattice constants are the same as those of the stage-1 structure, the simulated XRD pattern of stage 3 with the tetrahedral sites is summarized in table S3. Similarly, the *a*- and *b*-lattice constants of 2H-TaS_2 were used for the simulation pattern of stage 3 with octahedral sites as in table S4.

The diffraction intensity was enhanced at *002l* indexes. When these indexes were assigned to the obtained peaks, the *c*-lattice parameter was estimated to be 35.67 Å, as shown in table S1. Although other candidates of the stage structure such as stage 4, stage 5, and combinations of stage 2 and stage 4 were considered, as shown in figure S6, the stage-3 structure was the most likely crystal structure.

Besides, the total energies of stage-3 structure with tetrahedral and octahedral sites were compared in figure S7. When the concentration of Ag is 0.037 ($Ag_2Ta_{54}S_{108}$), the stage-3 structure with octahedral sites (−7.9330 eV/atom) is more stable than that with tetrahedral sites (−7.9295 eV/atom). Conversely, when x = 0.333 ($Ag_{18}Ta_{54}S_{108}$), the structure with tetrahedral sites (−7.5248 eV/atom) becomes more stable than that with octahedral sites (−7.4999 eV/atom). Among the many possible arrangements of Ag ions, these structures were selected as typical states with high and low Ag concentration. DFT calculations show that, when Ag concentration gets diluted, the total energy becomes almost the same, however the stage-3 structure with the octahedrons is slightly more stable. In this study, the Ag concentration in the stage-3 structure was experimentally obtained as ~ 0.1 from EDS measurements. It is difficult to know which structure is more stable at x = 0.1. Also, it was taken into consideration that, since the total energies are

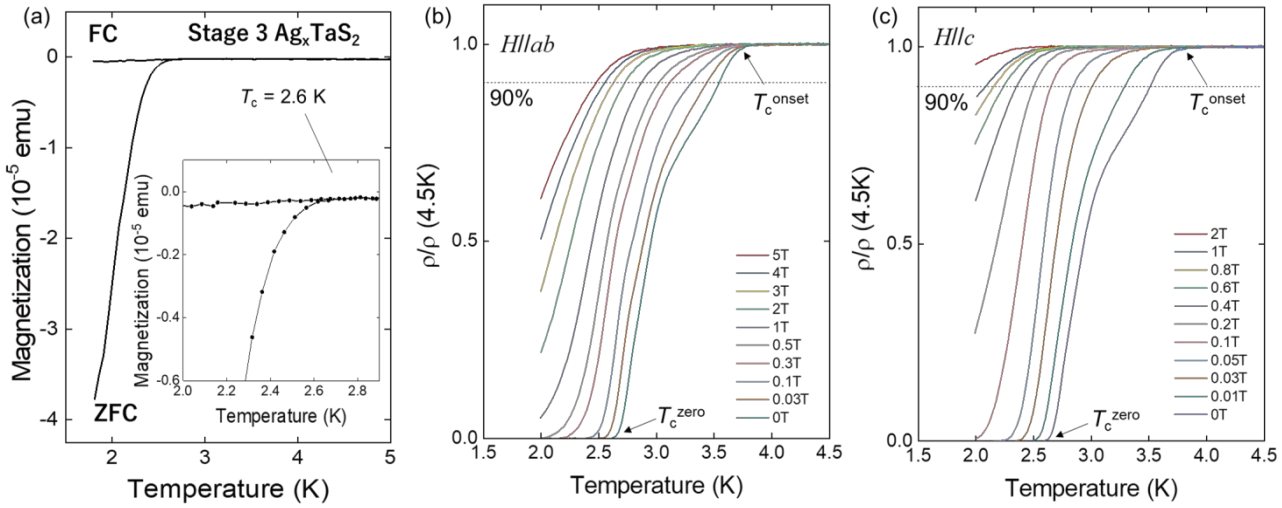

Figure 5. (a) Temperature dependence of magnetic susceptibility for Ag_xTaS_2 under 10 Oe. The inset shows the expanded view of temperature range between 2 and 3 K. (b)−(c) Temperature dependence of normalized resistivity [ρ(*T*)/ρ(4.5 K)] under magnetic field parallel with (b) *ab*-plane (*H//ab*) and (c) *c*-axis (*H//c*) for Ag_xTaS_2 with stage-3 structure. The dotted line denotes a criterion of 90% of the resistivity to determine the upper critical magnetic fields (H_{C2}).

almost comparable, the Ag ions may be able to occupy both sites during the process of migration in TaS_2 interlayers via the water-soaking process. Such structural instability could induce a distortion resulting in a broader XRD profile of stage 3. In figure S1 (a), the full width at half maximum of the main peak for the sample with stage-3 structure is four times larger than those of other single crystals. Also, the structural degradation could be as a result of the shift of TaS_2 layers, which occurs during the reformation from stage-2 to stage-3. As described above, the stacking rule makes the TaS_2 layers shift according to Ag migration. Such movements are likely to induce local distortion. These are potential reasons for the broad XRD profile of stage-3.

3.3 Superconducting properties

The superconducting transition of the stage-3-structured $Ag_{0.11}TaS_2$ was observed via the magnetic and electronic measurements. Figure 5 (a) shows the temperature dependence of the field-cooled (FC) and zero-field-cooled (ZFC) susceptibilities of the samples from 1.8 K to 5 K under 10 Oe. It was observed that the FC and ZFC curves separate at 2.6 K and the high-diamagnetic susceptibility originated from the bulk superconductivity. Figures 5 (b) and (c) show the temperature dependence of resistivity below 4.5 K under the magnetic fields along both orientations, *ab*-plane (*H//ab*), and *c*-axis (*H//c*), of the single-crystalline $Ag_{0.11}TaS_2$. To investigate the anisotropic properties, the ρ-T curves were normalized using the resistivity at 4.5 K. Herein, T_c^{onset} denotes the starting point of the decrease in resistivity from the normal conducting state, while T_c^{zero} denotes the point at which the line for zero resistivity crosses the ρ-T curve, as indicated in figures 5 (b) and (c). The T_c^{onset} and T_c^{zero} were obtained to be 3.7 and 2.6 K, respectively, without a magnetic field, and were found to decrease gradually with the increasing magnetic field. Furthermore, the suppression of the superconductivity with the magnetic field along the *H//c* direction was more obvious than that in the *H//ab* direction. This is the typical behavior of layered superconductors, which indicates high anisotropy.

To determine the upper-critical magnetic field (H_{C2}), a criterion of 90% of the resistivity was employed and the results for the two orientations are shown in figure 6. The

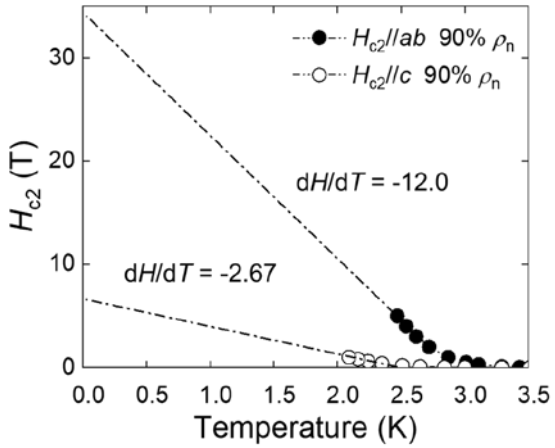

Figure 6. Temperature dependence of the upper critical magnetic field for Ag_xTaS_2 with stage-3 structure obtained from 90% of criterion in ρ-T curves. Solid and open circles denote H_{c2}//*ab* and H_{c2}//*c*, respectively. The dashed lines indicate the straight-line approximation.

value of H_{C2} at the zero temperature can be estimated from the temperature-dependent upper-critical magnetic field for type-2 superconductors using Werthamer–Helfand–Hohenberg (WHH) relation [33]:

$$H_c = -0.693 \times dH_c(T)/dT /_{T_c} \times T_c \quad (1)$$

The value of dH_{c2} $(T)/dT$ is obtained from the slope, as shown in figure 6. The superconducting parameters ($H_{c2}^{//ab}(0)$, $H_{c2}^{//c}(0)$, $\xi_{ab}(0)$, $\xi_c(0)$), and $\gamma(0)$ are summarized in Table 1, where ξ_{ab} (0) and ξ_c (0) are the coherence lengths along the *ab* plane and *c*-axis, respectively. They are obtained from the Ginzburg-Landau relation:

$$H_{c2}^{//ab} = \Phi_0 / 2\pi\xi_{ab}(0) \times \xi_c(0), H_{c2}^{//c} = \Phi_0 / 2\pi\xi_{ab}^2(0), \quad (2)$$

where Φ_0 is the quantum flux. The anisotropy of the upper-critical magnetic field (γ) is also estimated to be 5.2 from the following formula:

$$\gamma = H_{c2}^{//ab} / H_{c2}^{//c} \quad (3)$$

Table 1. Summary of superconducting parameters for the Ag_xTaS_2 with stage-3 structure

$dH_{c2}^{//ab}/dT$	$dH_{c2}^{//c}/dT$	$H_{c2}^{//ab}(0)$	$H_{c2}^{//c}(0)$	$\xi_{ab}(0)$	$\xi_c(0)$	$\gamma(0)$
−12.0 T/K	−2.67 T/K	23.9 T	4.57 T	26.8 nm	5.13 nm	5.2

4. Discussion

4.1 Relationship between CDW and superconductivity

The temperature dependence of the normalized resistivity for the reported Ag_xTaS_2 with stage-1 and stage-2 structure and obtained stage-3-structured Ag_xTaS_2 in this work were summarized in figure 7 [24]. Although the stage-1 structure shows two anomalies at 80 and 180 K, the anomaly at 80 K disappears in the stage-2 structure. The sample with the stage-2 structure has one anomaly at 170 K. These anomalies have been discussed in previous studies [19, 34]. Two anomalies at 80 and 180 K in stage-1 are first- and second-order transitions, respectively. The superlattice satellite (SLS) was also observed at 92 K in stage-1[19]. It is thought to be associated with the first-order transition. On the other hand, in a previous study [34], the *c*-lattice parameter continually decreases with cooling from room temperature, increases at 180 K afterward, and suddenly falls at 100 K. These structural transitions are in excellent agreement with the anomalies in resistivity, and their origins have been considered to be related to the order of arrangement of the Ag ions and/or CDW [34]. Although such an expansion of the *c*-axis is often observed for the formation of CDW [35, 36], direct evidence of CDW has not been obtained currently. Further investigations are necessary to understand the mechanism of their anomalies with the resistivity. Whereas, the SLS related to CDW of stage-2-structured Ag_xTaS_2 ($x < 0.26$) has been observed below ~85 K in previous studies [36, 37]. However, the accurate onset temperature for this CDW has not been revealed [37]. Also, the relationship between the anomaly at 170 K in resistivity and this observed CDW is yet to be reported.

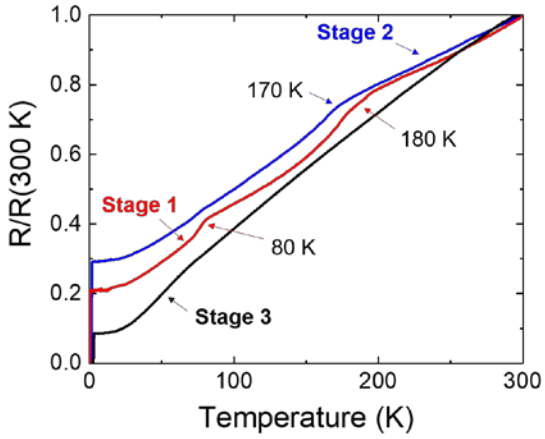

Figure 7. Temperature dependence of the normalized resistivity of Ag_xTaS_2 with stage-1 to stage-3 structures from 0 to 300 K.

On the other hand, no apparent anomaly was observed in the stage-3-structured Ag_xTaS_2. Although it is difficult to discuss whether the sample with stage-3 structure has CDW essentially or not from the resistivity measurements, at least the structural distortion, which was observed in the XRD measurement in figure S1(a), is expected to compete with the formation of CDW, thereby suppressing its formation in the stage-3-structured Ag_xTaS_2 [38]. The structural distortion could be attributed to two reasons. First, as described in section 3.2, the stacking rule makes the TaS_2 host layers shift according to the Ag migration. This reconstruction from stage 2 to stage 3 indicates a local distortion in figure S1(b). Second, the total energies of the stage-3 structures with tetrahedral and octahedral sites were almost comparable in figure S7. Therefore, the structural instability, according to the Ag positions between the octahedral and tetrahedral sites, is likely to occur during Ag migration. For the above reasons, the CDW observed in stage 2 should be suppressed in the process of forming a stage-3 structure by the deintercalation of Ag ions.

The CDW condenses the electrons and pins them at the lattice. Therefore, the suppressed CDW is widely acknowledged as the cause of the increase in the conduction electrons, as well as the ultimate enhancement in T_c, according to McMillan's theory [39]; the number of Cooper pairs increases by releasing free electrons. This concept qualitatively explains the resistivity behavior of stage 3. When suppressing CDW, the structural distortion in the stage-3 structure enhances T_c from 1.7 to 3.8 K.

The observed anomalies and T_cs are listed in table 2. Although there is a need to clarify the origin of these anomalies via transmission electron microscopy and

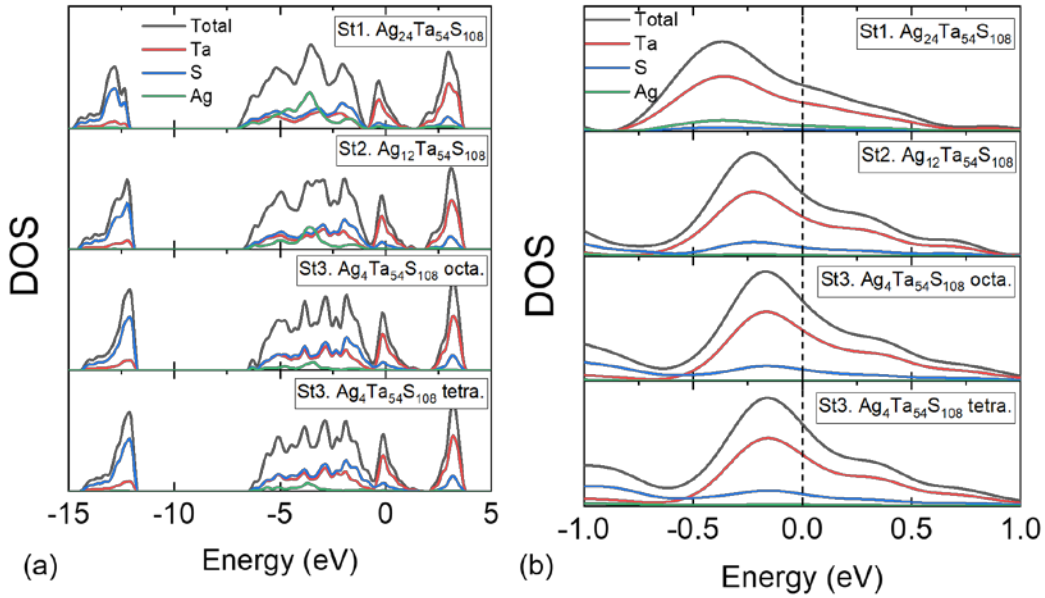

Figure 8. (a) DOS of $Ag_xTa_{54}S_{108}$ (x = 24, 12, 4) with different stage structures. Also the stage-3 structures with octahetral and tetrahedral sites were calculated respectively. (b) An expanded view of the DOS from -1.0 to 1.0 eV.

scanning tunnelling microscopy, these results are in good agreement with the known relationship between CDW and superconductivity.

Table 2. Summary of the onset of charge density wave order, superconducting transitions, and space group for the parent material (TaS_2), Ag_xTaS_2 with stage-1[24], stage-2[24], and stage-3 structures.

	TaS_2	St. 1	St. 2	St. 3
anomaly	78 K	80 K, 180 K	170 K	-
T_c	0.8 K	0.4 K	1.7 K	3.8 K
Space group	P 6_3/mmc	P 6_3/mmc	R-3m	P-6 m2(tet.) P3 m1(oct.)

4.2 Density of states in the stage structures

To understand the enhancement of T_cs, the DOSs of the Ag_xTaS_2 with different stage structures were calculated based on the DFT. 3 × 3 × 3, 3 × 3 × 1, and 3 × 3 × 1 supercells were modeled for the stage-1, -2, and -3 structures, respectively. Structural relaxations were performed on each supercell. Figures 8 (a) and (b) show the DOSs from −16 to 5 eV and the expanded view near the Fermi level, respectively. Although the Ag intercalation formed different crystal structures with different space groups, the electronic states did not show a significant difference among the series of stage structures, as shown in figure 8 (a). The electronic states can be regarded as a rigid band model, if electrons from the interfacial Ag ions gradually occupy the states of the conduction band. The calculated Fermi level in figure 8 (b) shifted to a higher energy level. The sloop of the DOS at the Fermi level is negative; hence, the number of conduction electrons need to be reduced with increasing Ag concentration, and superconductivity should be suppressed according to McMillan's theory. The DFT calculations can qualitatively explain the enhancement of superconductivity in the stage-3-structured Ag_xTaS_2.

Besides, calculations were performed to evaluate the Fermi surface by using a unit cell (1 × 1 × 1) shown in figure S3, to calculate without considering the folding into the first Brillouin zone. Afterward, the Fermi surface was shifted according to the Ag ion concentration, assuming a rigid band model, as shown in figure S4. Although it is difficult to discuss the actual Fermi surface quantitatively, these results are shown in figure S3 as a supplement.

5. Conclusions

We successfully realized the stage-3-structured Ag_xTaS_2, which was predicted 40 years ago, via the PDII method and water-soaking process. The developed stacking rule and DFT calculations provided two possible crystal structures with tetrahedral sites (P-6 m2) and octahedral sites (P3 m1). We discovered the superconductivity of this material manifested at 3.8 K. The upper-critical field and its anisotropy was also determined. Notable is the increase in superconducting transition temperature with an increasing number of stages despite the degradation of crystallinity in the stage-3 structure. In this work, the suppression of CDW and the increase in DOS at the Fermi level were suggested as possible reasons behind the experimental observation. Also, the suppression of CDW is thought to be caused by the structural instability of Ag positions between the tetrahedral

and octahedral sites and/or the local strain caused by the shift of TaS_2 layers during reformation from stage 2 to 3.

The findings in this work would motivate the development of further promising techniques for investigating different layered-TMDs, guest species, and stage structures. Structural diversity achieved by combining such components is expected to create new functional materials.

Acknowledgements

This work was supported by the Japan Society for the Promotion of Science (Grant No. 19F19039, 18K19122 and 19H02420), Japan Science and Technology Agency CREST (Grant No. JPMJCR19J1), the Cooperative Research Program of "Network Joint Research Center for Materials and Devices" and "the Dynamic Alliance for Open Innovation Bridging Human, Environment and Materials".

References

[1] Wenjuan Z, Tony L, Han W, Peide Y and Xiangfeng D 2019 Nanoscale electronic devices based on transition metal dichalcogenides *2D mater* **6** 032004

[2] Yijun Y, Fangyuan Y, Xia F L, Ya J Y, Cho Y H, Liguo M, Xiaohai N, Kim S, Son Y W, Donglai F, Siyan L, Cheong S W, Xian H C and Yuanbo Z 2015 Gate-tunable phase transitions in thin flakes of 1T-TaS_2 *Nat. Nanotechnol* **10** 270-276

[3] Mak K F and Shan J 2016 Photonics and optoelectronics of 2D semiconductor transition metal dichalcogenides *Nat. Photonics* **10** 216-226

[4] Guanxiong L, Bishwajit D, Pope T R, Salguero T T, Lake R K and Balandin A 2016 A charge-density-wave oscillator based on an integrated tantalum disulfide-boron nitride-graphene device operating at room temperature *Nat. Nanotechnol* **11** 845-850

[5] Thyveetil M A, Coveney P V, Greenwell H C and Suter J L 2008 Role of host layer flexibility in DNA guest intercalation revealed by computer simulation of layered nanomaterials *J. Am. Chem. Soc* **130** 12485-12495

[6] Mokaya R 2000 Novel layered materials: Non phosphates *Encyclopedia of Separation Science* **2003** 1610-1617

[7] Dresselhaus M S and Dresselhaus G 2002 Intercalation compounds of graphite *Adv. Phys* **51** 1-186

[8] Li Y, Lu Y, Adelhelm P, Titirici M M and Hu Y S 2019 Intercalation chemistry of graphite: alkali metal ions and beyond *Chem. Soc. Rev* **48** 4655-4687

[9] Wilson J A, DiSalvo F J and Mahajan S 1975 Charge-density waves and superlattices in the metallic layered transition metal dichalcogenides *Adv.Phys* **14** 117-201

[10] Meyer S F, Howard R E, Stewart G R, Geballe T H and Acrivos J V 1975 Properties of intercalated 2H-$NbSe_2$, 4Hb-TaS_2 and 1T-TaS2 *J. Chem. Phys* **62** 4411-4419

[11] Hayashi K and Kawamura A 1986 Formation of TaS_2 Polytypes and Hydrogen Impurity *Mater. Res. Bull* **21** 1405-1410

[12] DiSalvo F J, Bagley B G, Voorhoeve J M and Waszczak J V 1973 Preparation and properties of a new polytype of tantalum disulfide (4Hb-TaS_2) *J. Phys. Chem. Solids* **34** 1357-1362

[13] Sugai S 1985 Lattice vibrations in the charge-density wave states of layered transition metal dichalcogenides *Phys. Solidi B* **129** 13-39

[14] Harper J M E, Geballe T H and DiSalvo F J 1977 Thermal properties of layered transition-metal dichlcogenides at charge-density-wave transitions *Phys.Rev. B* **15** 29432951

[15] Sankar R, Peramaiyan G, Muthuselvam I P, Wen C Y, Xiaofeng X and Chou F C 2018 Superconductivity in a misfit layered $(SnS)_{1.15}(TaS_2)$ *Compound. Chem. Mater* **30** 1373-1378

[16] Jochen S and Robert S 1987 Electrochemical formation of Ag_xTiS_2 at 300K *Solid State Ion* **23** 197-202

[17] Scholz G A 1993 Ag_xTaS_2 single crystals: silver diffusion, activation energies and the potentiometric method *Solid State Ion* **62** 235-242

[18] Gerards A G, Roede H, Haange R J, Boukamp B A and Wiegers G A 1988 Kinetic properties of intercalates Ag_xTaS_2 *Solid State Ion* **27** 73-80

[19] Boebinger G S, Wakefield N I F, Marseglia E A, Friend R H and Tatlock G J 1983 Transport and structural properties of the silver intercalation complexes of 2H-TaS_2 *Physica* **117/118B** 608-610

[20] Wiegers G A, Bouwmeester and Gerards A G 1985 Stability, staging and ordering in silver intercalates of 1T-TiS_2, 2H-NbS_2 and 2H-TaS_2 *Solid State Ion* **1** 155-162

[21] Ramos C, Lerf A, Saibene S and Butz T 1988 The mixed conductor $Ag_{2/3}TaS_2$: in situ monitoring of electrointercalation and silver mobility *Solid State Ion* **31** 177-185

[22] Van de Berg J. M, Thesis (University of Leiden, The Netherlands, 1964)

[23] Scholz G.A and Frindt R F 1980 Structure and staging of intercalated Ag_xTaS_2 and Ag_xTiS_2 *Mat. Res. Bull* **15** 1703-1716

[24] Fujioka M, Kubo N, Nagao M, Msiska R, Shirakawa N, Demura S, Sakata H, Kaiju H and Nishii J 2018 Superconductivity in Ag_xTaS_2 single crystals with stage structure obtained via proton-driven ion introduction *J. CERAM. SOC. JPN* **126** 963-967

[25] Fujioka M, Wu C, Kubo N, Zhao G, Inoishi A, Okada S, Demura S, Sakata H, Ishimaru M, Kaiju H and Nishii J 2017 Proton-driven intercalation and ion substitution utilizing solid-state electrochemical reaction *J. Am. Chem. Soc* **139** 17987-17993

[26] Kresse G and Furthmüller J 1996 Efficient iterative schemes for ab initio total-energy calculations using a plane-wave basis set *Phys. Rev. B* **54** 11169-11186

[27] Kresse G and Hafner J 1993 Ab initio molecular dynamics for liquid metals *Phys. Rev. B* **47** 558-561

[28] Grimme S, Antony J, Ehrlich S and Krieg S 2010 A consistent and accurate an initio parameterization of density functional dispersion correction (DFT-D) for the 94 elements H-Pu *J. Chem. Phys.* **132** 154104

[29] Grimme S, Ehrlich S and Goerigk L 2011 Effect of the damping function in dispersion corrected density functional theory *J. Comp. Chem*. **32** 1456

[30] Perdew J P, Burke K and Ernzerhof M 1996 Generalized gradient approximation made simple *Phys. Rev. Lett* **77** 3865-3868

[31] Eisenberg D and Kauzmann W 1969 *The structure and properties of water (* Oxford University Press)

[32] Momma K and Izuni F 2011 VESTA 3 for three-dimensional visualization of crystal, volumetric and morphology data *J.Appl.Crystallogr* **44** 1272-1276

[33] Werthamer N R, Helfand E and Hohenberg P C 1966 Temperature and purity dependence of the superconducting critical field, H_{c2}. III. electron spin and spin-orbit effects *Phys. Rev. B* **147** 295-302

[34] Scholz G A and Frindt R F 1983 Electrical resistivity of silver intercalated 2H-TaS_2 *Phys. Stat. Sol* **79** 483-488

[35] Scholz G A, Frindt R F and Curzon A E 1982 Electron diffraction investigation of the Ag_xTaS_2 system (I) *Phys. Stat. Sol* **71** 531-542

[36] Scholz G A, Frindt R F and Curzon A E 1982 Electron diffraction investigation of the Ag_xTaS_2 system (II) *Phys. Stat. Sol* **72** 375-390

[37] Scholz G A, Singh O, Frindt R F and Curzon A E 1982 Charge density wave commensurability in 2H-TaS_2 and Ag_xTaS_2 *Solid State Commun* **44** 1455-1459

[38] Wagner K E, Morosan E, Hor Y S, Tao J, Zhu Y, Sanders T, McQueen T M, Zandbergen H W, Williams A J, West D V and Cava R J 2008 Tuning the charge density wave and superconductivity in Cu_xTaS_2 *Phys. Rev. B* **78** 104520-1-104520-6

[39] Gabovich A M, Voitenko A I and Ausloos M 2002 Charge- and spin-density waves in existing superconductors: competition between Cooper pairing and Peierls or excitonic instabilities *Phys. Rep* **367** 583-709